

Supporting Information

Insight of the preponderant role of the lattice size in the Sn-based colusite for promoting high power factor

Paulina Kamińska^a, Cédric Bourgès^{b*}, Raju Chetty^b, Daniel Gutiérrez-Del-Río^b, Piotr Śpiewak^a,
Wojciech Świążkowski^a, Toshiyuki Nishimura^c, Takao Mori^{b,d*}

^a *Materials Design Division, Faculty of Materials Science and Engineering, Warsaw University of Technology, Wołoska 141, 02-507 Warsaw, Poland*

^b *WPI International Center for Materials Nanoarchitectonics (WPI-MANA), National Institute for Materials Science (NIMS), Namiki 1-1, Tsukuba, 305-0044, Japan*

^c *Research Center for Structural Materials, National Institute for Materials Science (NIMS), Namiki 1-1, Tsukuba, 305-0044, Japan*

^d *Graduate School of Pure and Applied Sciences, Tsukuba University, Tennoudai 1-1-1, Tsukuba 305-8671, Japan*

Corresponding authors: BOURGES.Cedric@nims.go.jp; MORI.Takao@nims.go.jp

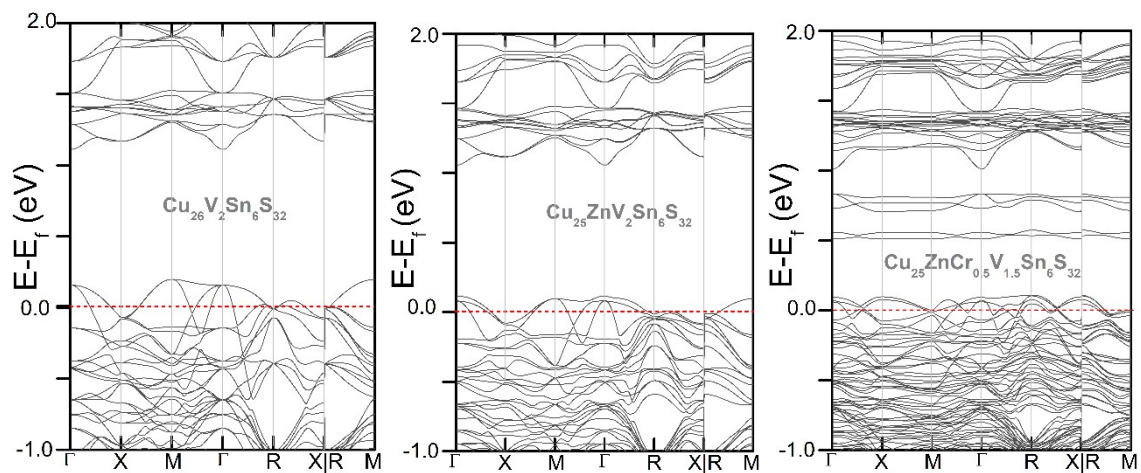


Figure S1. Electronic band structures of $\text{Cu}_{26}\text{V}_2\text{Sn}_6\text{S}_{32}$, $\text{Cu}_{25}\text{ZnV}_2\text{Sn}_6\text{S}_{32}$, and $\text{Cu}_{25}\text{ZnCr}_{0.5}\text{V}_{1.5}\text{Sn}_6\text{S}_{32}$

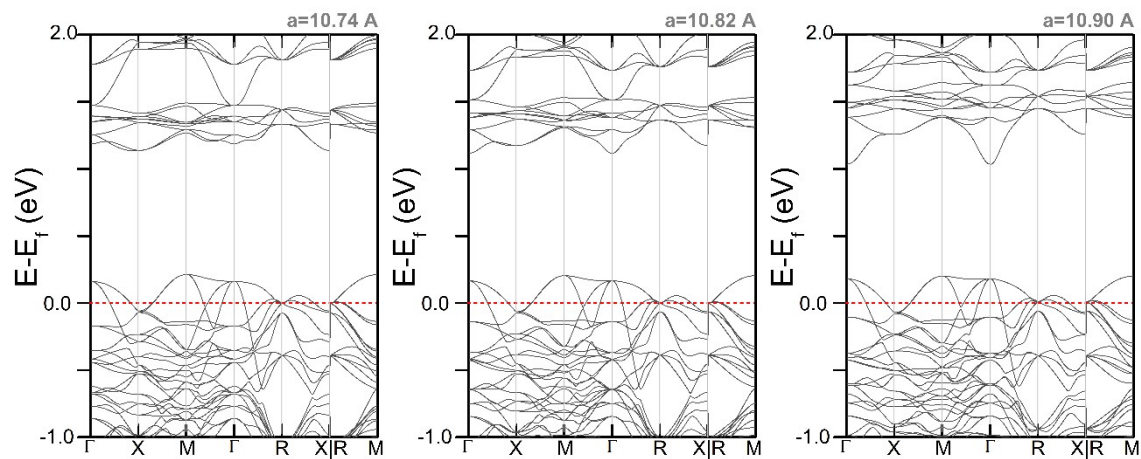


Figure S2. Electronic band structures and density of states (DOS) of $\text{Cu}_{26}\text{V}_2\text{Sn}_6\text{S}_{32}$ assuming different lattice parameters a (10.74 Å, 10.82 Å, and 10.90 Å)

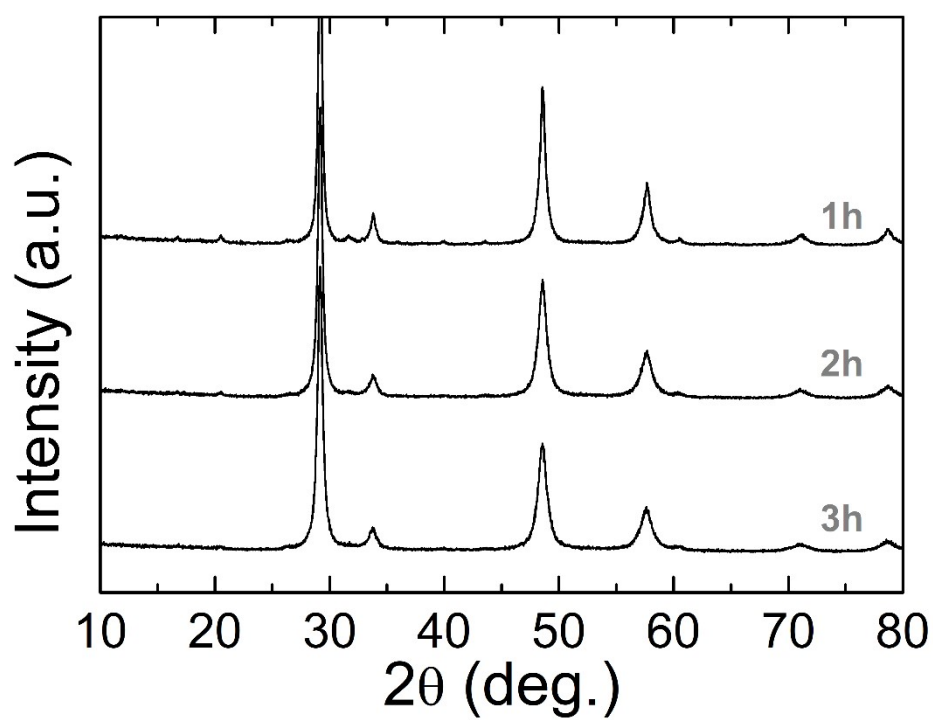


Figure S3. Powder X-ray diffraction patterns of $\text{Cu}_{25}\text{ZnV}_2\text{Ge}_6\text{S}_{32}$ compounds ball milled for a different time

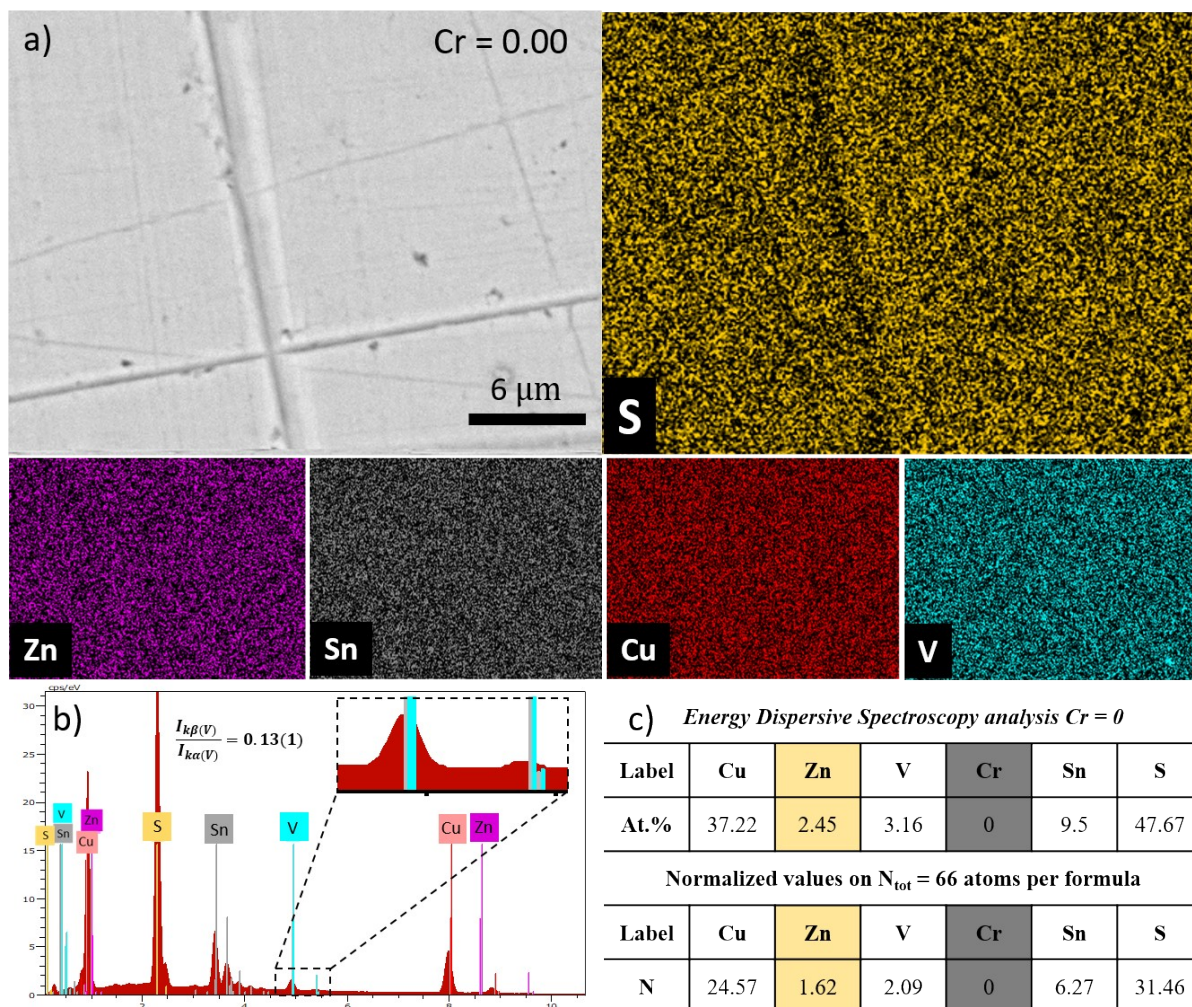


Figure S4. Energy dispersive spectroscopy analysis results on the polished surface of the $Cu_{25}ZnV_2Sn_6S_{32}$ sample sintered by SPS with a) EDS mapping b) its corresponding spectrum, and c) calculated atomic compositions

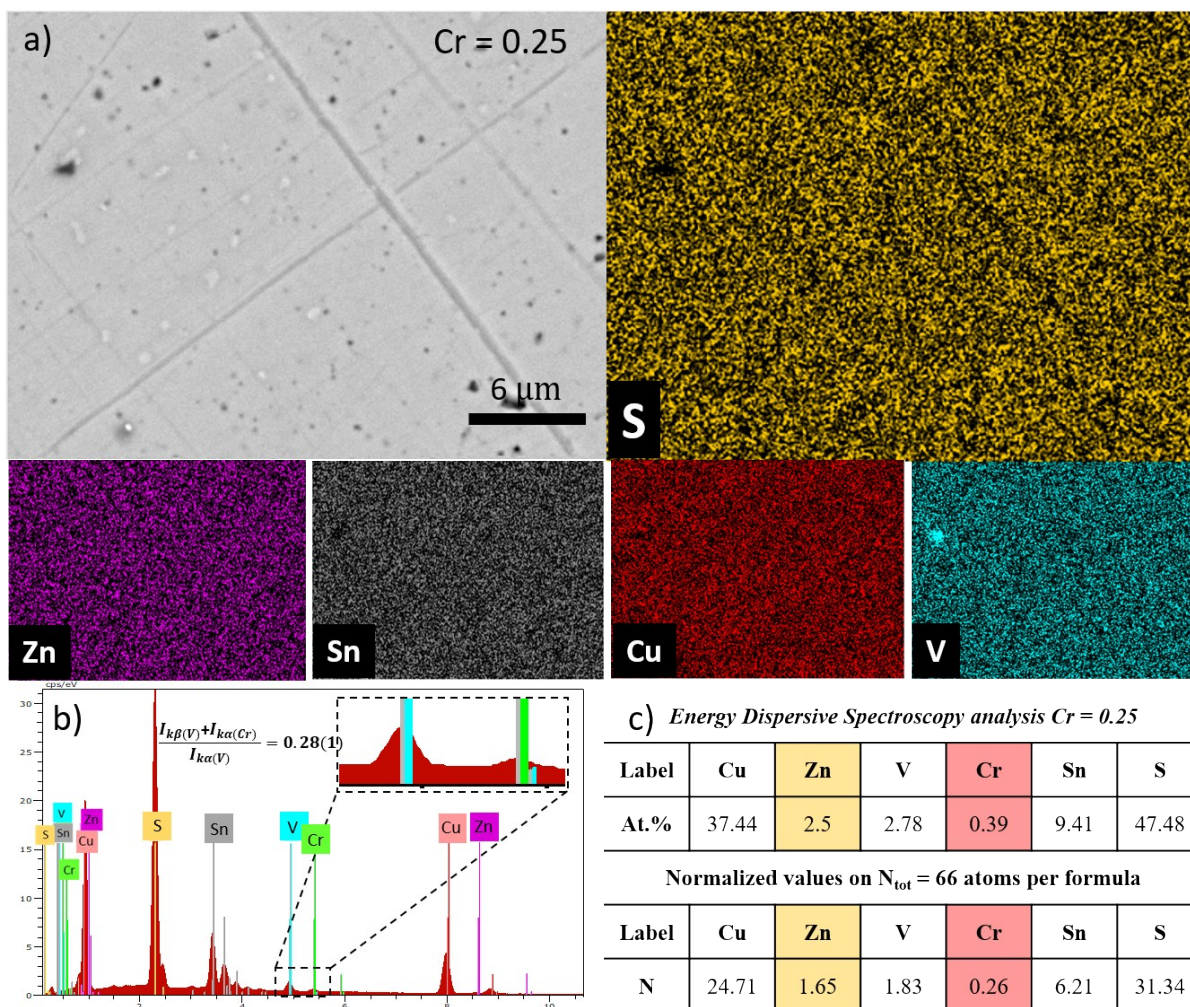


Figure S5. Energy dispersive spectroscopy analysis results on the polished surface of the $Cu_{25}ZnV_{1.75}Cr_{0.25}Sn_6S_{32}$ sample sintered by SPS with a) EDS mapping b) its corresponding spectrum, and c) calculated atomic compositions

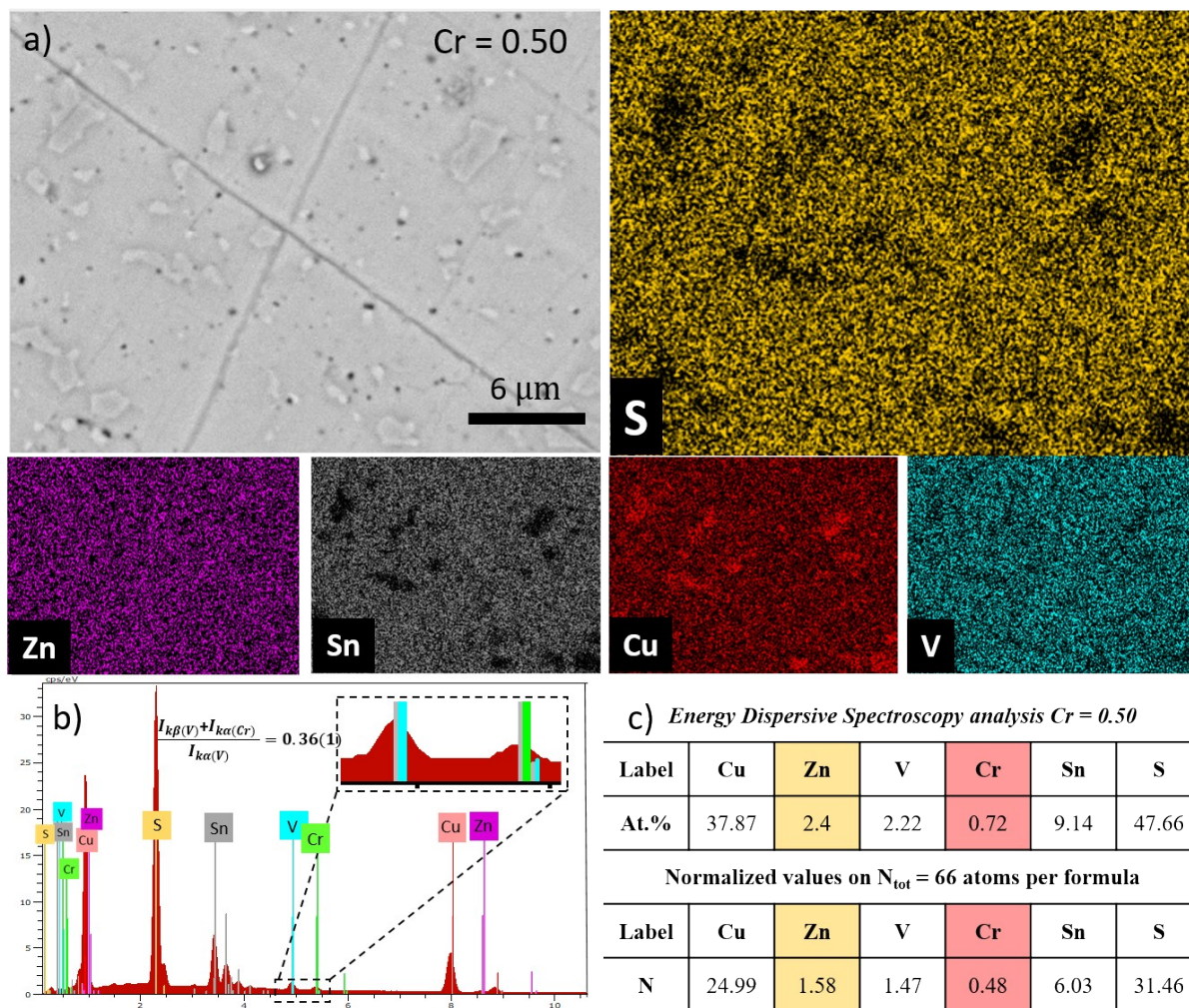


Figure S6. Energy dispersive spectroscopy analysis results on the polished surface of the $Cu_{25}ZnV_{1.5}Cr_{0.5}Sn_6S_{32}$ sample sintered by SPS with a) EDS mapping b) its corresponding spectrum, and c) calculated atomic compositions

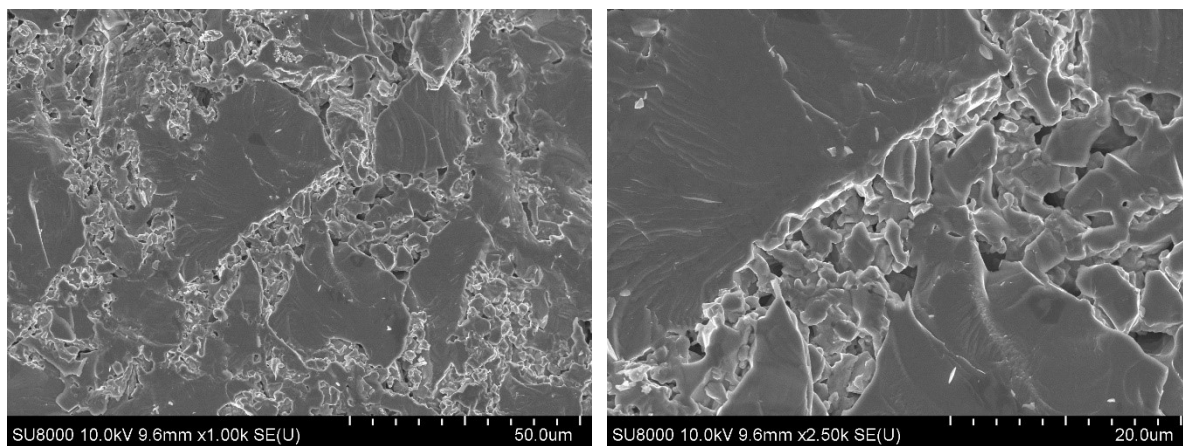


Figure S7. SEM images of a fractured surface of $\text{Cu}_{25}\text{ZnV}_2\text{Sn}_6\text{S}_3$ without ball milling step during the fabrication process

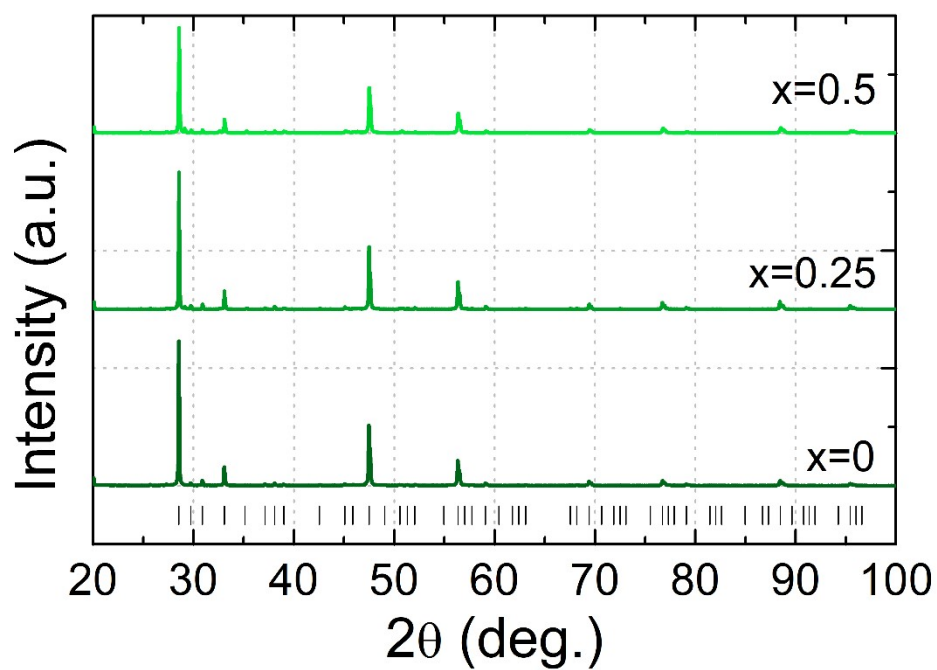


Figure S8. Powder X-ray diffraction patterns of sintered $\text{Cu}_{25}\text{ZnV}_{2-x}\text{Cr}_x\text{Sn}_6\text{S}_{32}$ compounds by hot-pressing

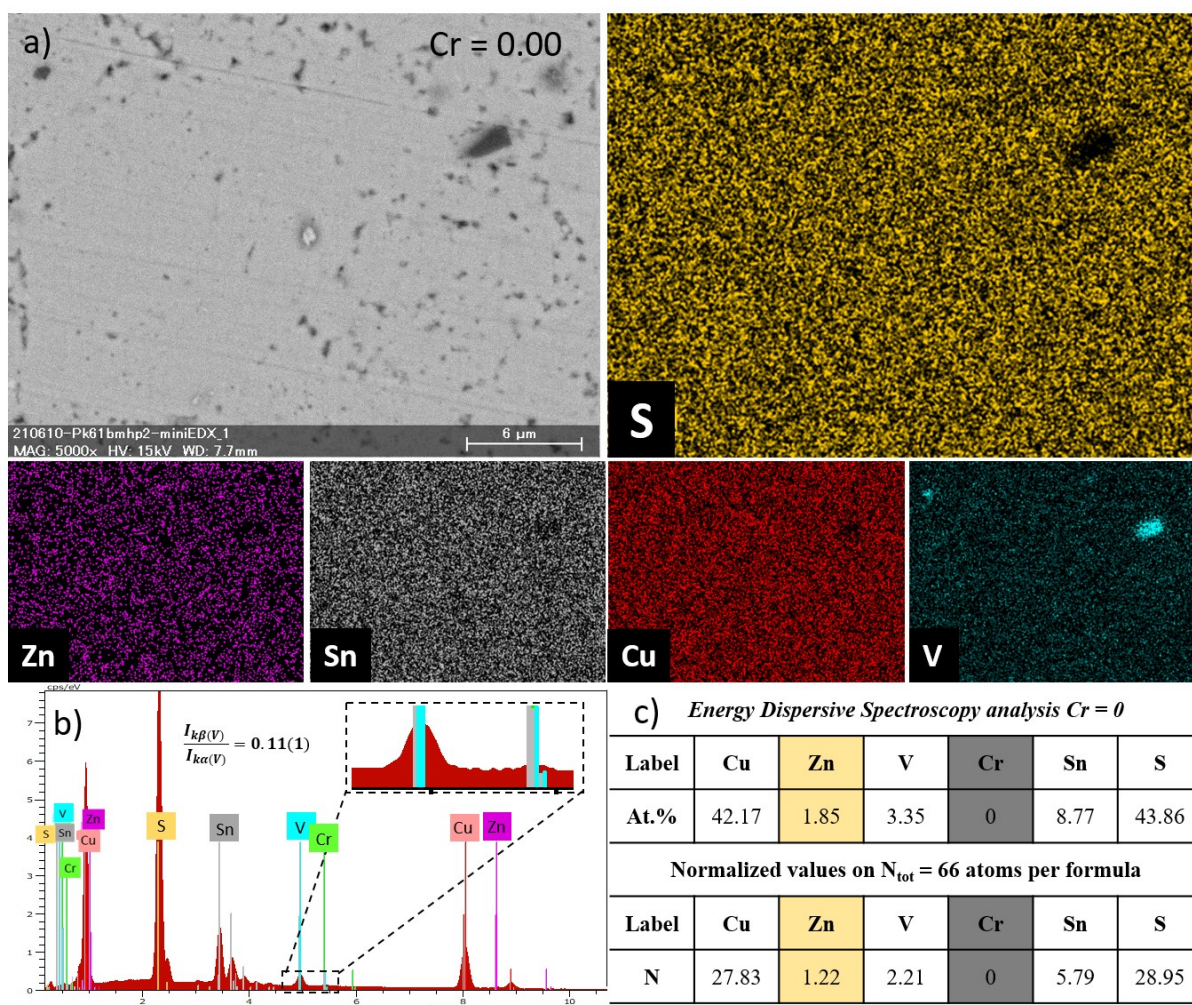


Figure S9. Energy dispersive spectroscopy analysis results on the polished surface of the $Cu_{25}ZnV_2Sn_6S_{32}$ sample sintered by hot-pressing with a) EDS mapping b) its corresponding spectrum, and c) calculated atomic compositions

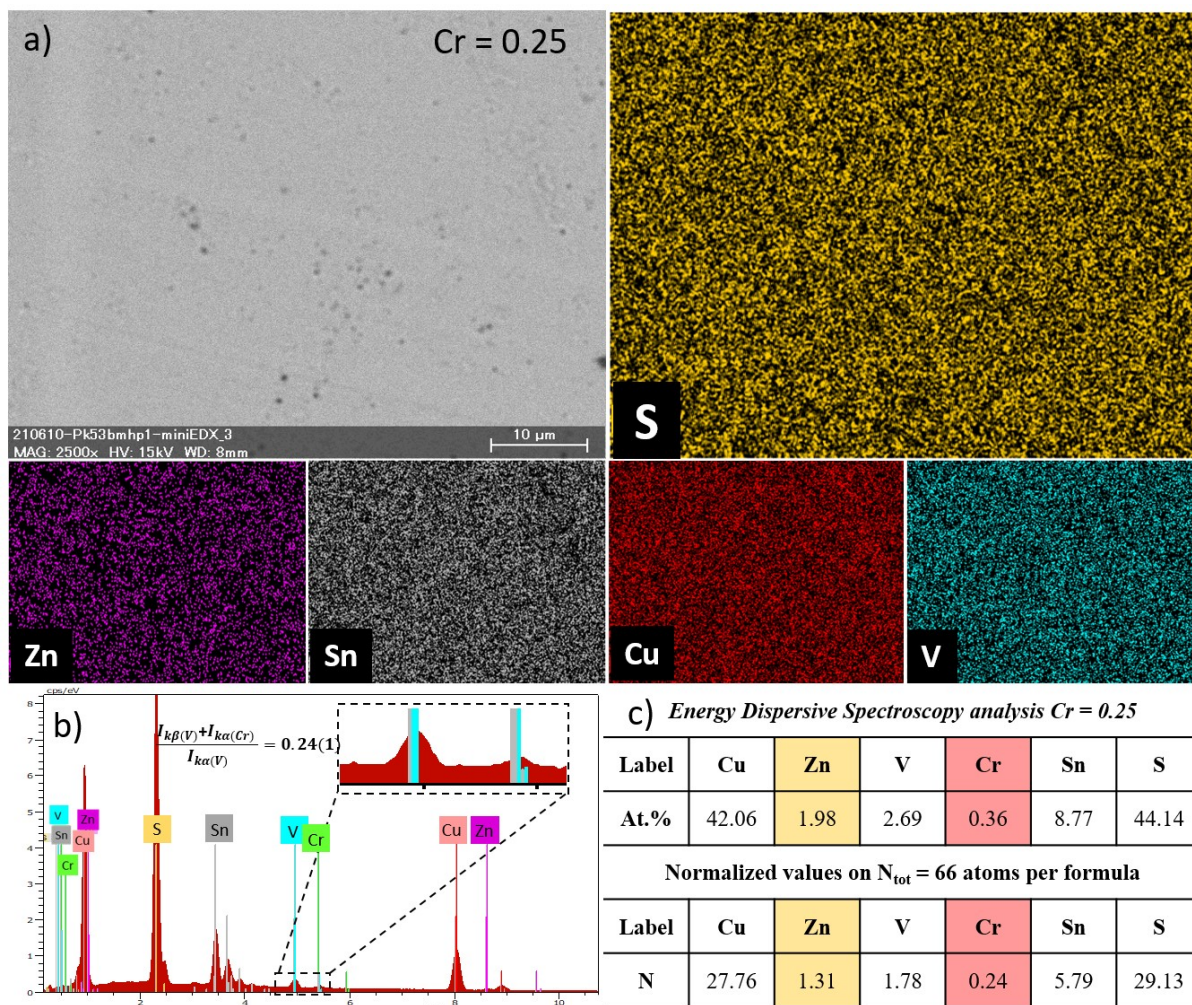


Figure S10. Energy dispersive spectroscopy analysis results on the polished surface of the $\text{Cu}_{25}\text{ZnV}_{1.75}\text{Cr}_{0.25}\text{Sn}_6\text{S}_{32}$ sample sintered by hot-pressing with a) EDS mapping b) its corresponding spectrum, and c) calculated atomic compositions

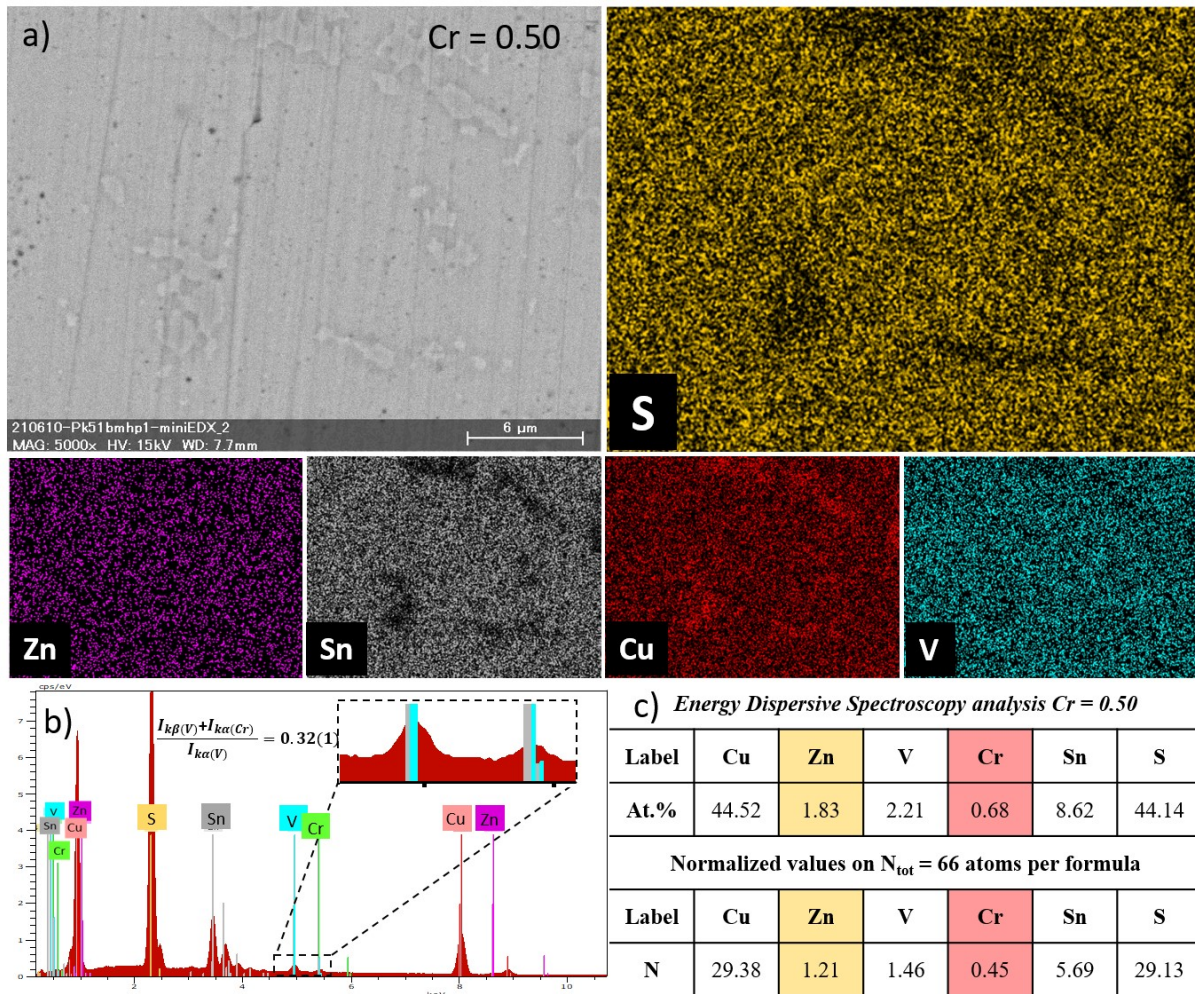


Figure S11. Energy dispersive spectroscopy analysis results on the polished surface of the $\text{Cu}_{25}\text{ZnV}_{1.75}\text{Cr}_{0.25}\text{Sn}_6\text{S}_{32}$ sample sintered by SPS with a) EDS mapping b) its corresponding spectrum, and c) calculated atomic compositions

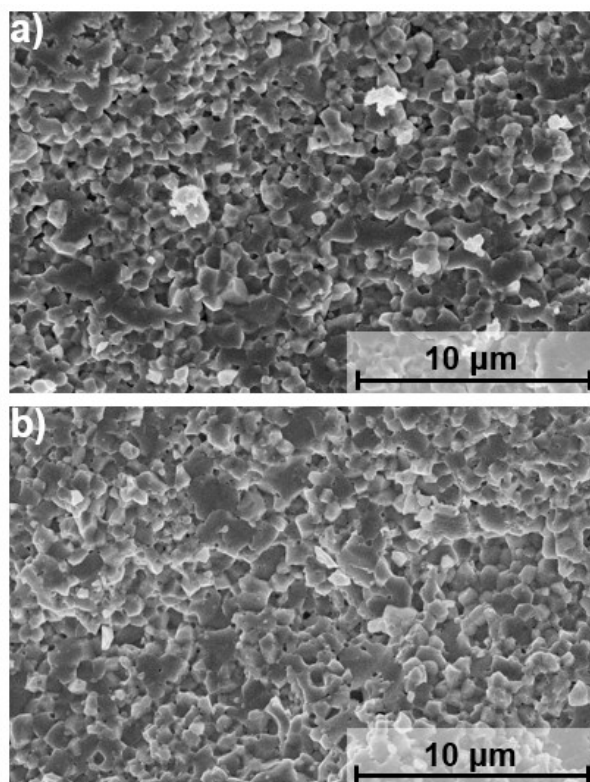


Figure S12. SEM images of a fractured surface of the hot-pressed $\text{Cu}_{25}\text{ZnV}_{2-x}\text{Cr}_x\text{Sn}_6\text{S}_{32}$ (a) $x = 0$, (b) $x = 0.5$.